JMEPEG (2011) 20:341–347
DOI: 10.1007/s11665-010-9710-5

1059-9495/$19.00

Numerical Simulation and Superplastic Forming of Ti-6Al-4V Alloy for a Dental Prosthesis

Xiaomei Li and Steven Soo

(Submitted March 25, 2010; in revised form June 2, 2010)

This article investigates superplastic forming (SPF) technique in conjunction with finite element (FE) simulation applied to dental repair. The superplasticity of Ti-6Al-4V alloys has been studied using a uniquely designed five-hole test with the aim of obtaining the modeled grain size and the flow stress parameters. The data from the five-hole test are subsequently put into the FE program for the simulation of a partial upper denture dental prosthesis (PUD4). The FE simulation of the PUD4 is carried out to set up appropriate input parameters for pressing due to the SPF process being fully automatic controlled. A variety of strain rates ranging from 2.4×10^{-5} to 1×10^{-3} s^{-1} are selected for the characterization of superplastic properties of the alloy. The Superflag FE program is used to generate an appropriate pressure-time profile and provide information on thickness, grain size, and grain growth rate distribution. Both membrane elements and solid elements have been adopted in the simulation and the results from both types of elements are compared. An evaluation of predicted parameters for the SPF of the prosthesis is presented.

Keywords dental prosthesis, finite element simulation, superplastic forming

1. Introduction

Superplastic forming (SPF) technology has been traditionally used in the aerospace industry by adapting the materials with superplastic properties into complex shapes through large deformation caused either by thermal cycling or internal stress (Ref 1-4). Some recent developments, exploiting its applications in dentistry, indicate that it can be used to produce a range of dental prostheses, provided that the superplastically formable material meets the requirements for weight, strength, and biocompatibility. Over the last decade, there has been increasing interest in the use of Ti-6Al-4V alloy in producing medical and dental device by the SPF technique because this type of alloy is biocompatible, light with high strength and good superplasticity (Ref 5-9).

The manufacture of superplastically forming components requires well-defined loading conditions (forming temperature, pressure-time profile) as well as accurate geometrical dies. The general mechanisms of deformation during forming can be described by three regions: diffusional creep, superplasticity, and power law creep. The flow stress is dependent on strain rate in a manner whereby it increases with increasing strain rate. The most common constitutive equation to describe SPF behavior is the so-called material power law or simple *K-m* model (Ref 10):

$$\sigma = K\dot{\varepsilon}^m, \quad \text{(Eq 1)}$$

where K is a material constant and m is the strain rate sensitivity. This model may have apparent limiting constraints when large deformation with complex geometry occurs and long forming times are required, since it does not take microstructural evolution into account and assumes that the mechanical properties remain constant during forming. The Mosher and Dawson model (Ref 11), on the other hand, emphasizes the significant role of α phase grain size and its growth as a function of time and strain on the material's superplastic behavior. In the present work, the Mosher and Dawson model has been adopted to describe the superplastic behavior of Ti-6Al-4V alloy and it takes the generic form:

$$\sigma = \Phi(\dot{\varepsilon}, T, g), \quad \text{(Eq 2)}$$

where T is the forming temperature and g is the grain size. Detailed formulations of the Mosher and Dawson model are available elsewhere (Ref 11).

Traditionally the SPF process has been mostly driven by empirical measurements. These are time consuming. In order to eliminate the need for such repetitive experiments and make the maximum benefits of SPF, an appropriate simulation of the SPF process is necessary. Finite element (FE) analysis has proven to be an efficient tool to simulate the superplastic behavior of Ti-6Al-4V alloy, and much progress has been made toward the optimization of sheet thickness, grain growth evolution, and loading conditions (Ref 12-15). For instance, Cheong et al. simulated grain size gradients in SPF of a Ti-6Al-4V engineering component using the commercial FE solver, ABAQUS (Ref 12). Pitt and Ramulu investigated the influence of grain size and microstructures of Ti-6Al-4V alloys under SPF conditions (Ref 13). However, there have been very few reports of SPF for dental applications.

The objective of the present work is to characterize Ti-6Al-4V alloys to be used in the fabrication of dental prosthesis and to experimentally investigate the superplasticity of this type of

Xiaomei Li, School of Materials Science and Engineering, Southeast University, Nanjing 211189, People's Republic of China; and **Steven Soo**, Dental Institute, King's College London, University of London, London SE1 9RT, UK. Contact e-mails: xmli6@seu.edu.cn and xmli888@yahoo.co.uk.

alloy by means of a specially designed five-hole test. FE simulations of a partial upper denture base have been carried out using the Superflag FE program. An evaluation of the predictions for the SPF process of dental prosthesis is presented.

2. Experimental Procedures

2.1 Materials

Ti-6Al-4V alloy was used in the SPF. The alloy is in disc shape with a diameter of 140 mm and a thickness of 0.5, 0.7, 1, and 3 mm, respectively. The approximate chemical composition was as follows: 0.08 C, 0.05 N, 0.20 O, 0.015 H, 5.50-6.75 Al, 3.5-4.5 V, Ti. The mechanical properties are shown in Table 1.

For superplastic pressing two types of dies were used, one was a steel die for the five-hole test, and the other was a die consisting of a steel ring and dental casting investment material (see Fig. 1). The selection of the ceramic die material is important in terms of its strength, thermal properties, and cost. Improper use of these die materials will lead to a failure of the die and perforation of the sheet during forming. About 1 kg of investment material (Croform WB), fully mixed with water, in the proportion of 100/12, was poured into the mold. Care was taken to ensure that the die was at the suitable height in the mold and in complete contact with a steel base.

2.2 Electron Microscopy

SEM experiments were carried out to reveal the grain structure of the sheet in the as-received condition, as well as revealing the microstructural evolution after forming. For the latter, two regions of the formed sheet were selected: one in the flat area and the other at the apex of the largest dome. An examined section was cut parallel to the rolling direction and short transverse plane (R-S plane). R denotes the rolling direction, L denotes the long transverse, and S denotes the short transverse. SEM samples were ground and polished to a final finish of 1 μm. Scratch free samples were subsequently etched in a mixture of HF and HNO_3 solution for a few seconds. The grain size of α phase was measured by the mean intercepts method (60-80 grains on average) from SEM micrographs. The SEM facility was a JEOL JSM-T220A and the secondary electron mode was used for imaging.

2.3 SPF Pressing

SPF experiments included material characterization testing and the forming of prostheses. A five-hole forming test was designed to characterize the superplasticity of Ti-6Al-4V alloys. The test was conducted based on a free forming approach and simply using an argon gas pressure cycle to "blow" the titanium sheet into five holes of different radii. The flow stress function of strain rate was derived from the biaxial multi-dome tests by taking the simple *K*-*m* model, as described in Eq 1. The constant *K* and *m* were obtained from the comparison of experimentally measured dome heights with a number of FE-SPF simulations, and in this study, the values of *K* and *m* were 338.06 (MPa s) and 0.425, respectively (Ref 8). The advantages of a multi-hole forming test over the conventional tensile test include shorter testing times, efficient use of equipment and closer to real forming of components (Ref 16). The aim of using the five-hole test was to determine constitutive parameters for the pressure cycle calculations. The modeled initial grain size and the target flow stress (or strain rate) from the simulations were used in the simulation of the dental prosthesis. The SPF pressing was performed at 900 °C using a 20-ton hydraulic press with argon gas pressure and computer monitoring software (Ref 8). A metallic die with five cylindrical holes was made, and the radii of the five holes were 8.50, 9.56, 10.63, 11.69, and 12.75 mm, respectively (Fig. 1a). The die was enclosed in an induction-heated furnace chamber and the temperature was raised to about 800 °C, when the titanium disc sheet could be inserted. Then the temperature was further raised up to the forming temperature 900 °C, and a clamping pressure of 6 tons was applied along with the gas pressure above the titanium sheet that is in accordance with the pressure-time cycle. The pressure profile was initially generated by an empirical guess of flow stress, and the radius of the middle hole was used for the calculation. Prior to the SPF experiments, the discs were carefully cleaned and the edge of the disc sheet was coated using boron nitride before being placed onto the steel die such that it could be readily extracted at the temperature of 700-800 °C. After forming, the depth of the five holes was measured and compared with the simulation results.

For the prostheses pressing, identical operating procedures were applied, but different dies were used. The die was formed using a steel ring and the phosphate-bonded investment material (Fig. 1b). The pressing was performed using a pressure profile obtained from the FE simulation. Examples of SPF work pieces of five hole bulging surfaces and dental prostheses are shown in Fig. 2.

2.3.1 Surface Reconstruction. In order to simulate the SPF of Titanium alloy sheet to produce the prosthesis, the surface of the dental master model, which had been waxed-up beforehand, needed to be scanned and the image was processed. A laser scanner (3DD Model 100, 3dd Digital Corp

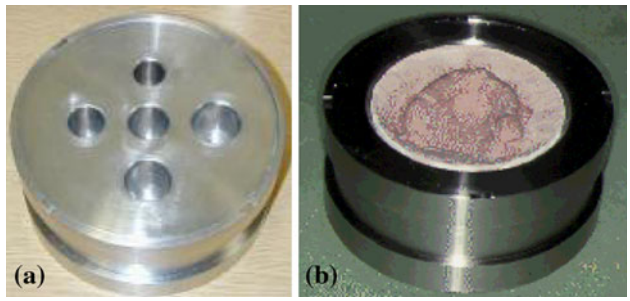

Fig. 1 The dies for superplastic forming: (a) steel die and (b) ceramic die

Table 1 Mechanical properties of Ti-6Al-4V alloy

Temperature range, °C	Strain rate range, s^{-1}	Stress range, MPa	Elongation, %	Yield strength, MPa	UTS, MPa
790-940	0.0001-0.001	5-30	Up to 1400	880	960

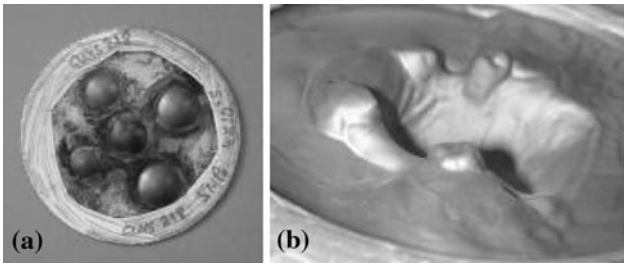

Fig. 2 Examples of superplastic forming pieces. (a) External surface of five-hole test and (b) internal surface of partial upper denture base

Laser Scanner) was employed and the surface of the dental master model was reconstructed in the computer. Seven to 10 scans were usually needed from a variety of angles to obtain an accurate reproduction of the complete surface. The stored patches were processed by deleting spikes and singularities and merged into a triangular meshed shell. Care was taken to ensure that the surface was completed without discernible holes before exporting the file for further processing. Subsequently, Paraform software from Digital Form Development™, providing excellent processing capabilities was used to merge the scanned surface with a virtual copy of the rim of the steel ring, to decimate elements to obtain an appropriate mesh size for FE simulation and remove any remaining mesh defects, such as holes. An input file for FE simulation was prepared from the output.

2.3.2 Finite Element Simulation. FE simulation software named "Superflag" was used to simulate the SPF processing of Ti alloys and dental prostheses (Ref 17). The program uses die surface reconstructions and meshes for the titanium sheet generated in the form of membrane elements or solid elements. Three-dimensional (3D) simulation of SPF of the five-hole test and of a prosthesis using membrane elements and solid elements were carried out with provision of information on thickness distribution, grain size evolution, stress output, and accuracy estimation (contact details between sheet and die). The accuracy estimation simply means a measure of how well a contact is established. Since SPF process is like blowing a bubble, blowing too hard produces high strain rate and high stress and the bubble will burst, while blowing too soft and the bubble will form slowly or not at all. Simulation is dominated by a number of factors that include target strain rate, stress, rate of energy dissipation, and material properties, e.g., initial grain size, grain growth evolution mechanisms, etc. In this study, both membrane elements and solid elements were used for the FE simulation of five-hole tests and prostheses. More details concerning these simulations will be presented in the following section.

3. Results and Discussion

3.1 Microstructural Examination

An SEM analysis was performed on the as-received Ti-6Al-4V alloy sheet (1-mm thick) as well as on the superplastically formed sheet tested at a strain rate of 2.4×10^{-5} s^{-1}. This target strain rate was selected from six different strain rates, based on the simulations which showed the optimal

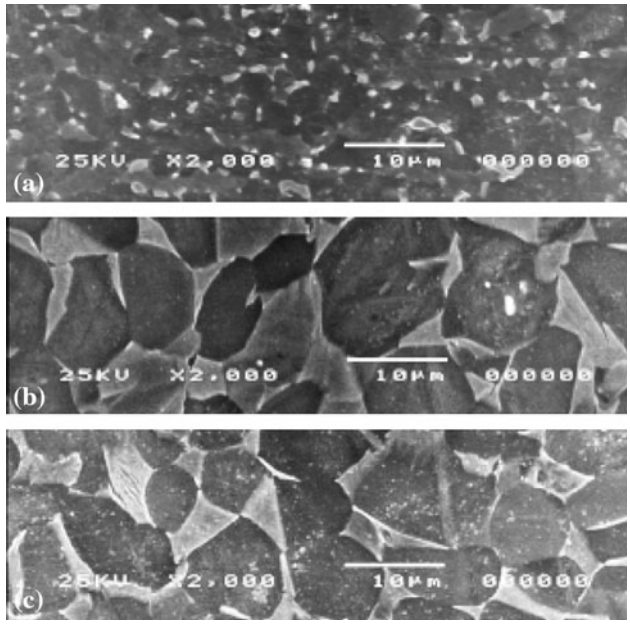

Fig. 3 SEM images of Ti-6Al-4V alloys, showing grain structure and two phases: α dark gray, β light gray. 1-mm thick, R-S section. (a) As received; (b) flat region, after forming at 900 °C, 2.4×10^{-5} s^{-1}; and (c) apex of the largest dome, after forming at 900 °C, 2.4×10^{-5} s^{-1}

superplastic behavior of the material. Since superplasticity is very sensitive to strain rate, which is used to produce pressure cycle, an inappropriate pressure profile can rapidly lead to perforation or incomplete adaptation at the end of the process. The microstructure of the as-received sheet and the microstructural evolution after forming at 900 °C is presented in Fig. 3. It was observed that the Ti-6Al-4V alloy contained two phases, i.e., α phase (dark gray) and transformed β phase (light gray). The alloy had a very fine-grain structure, and the α grains displayed clear grain boundaries with a measurable grain size of 3.17 µm. After forming at 900 °C, the grains grew significantly with a final grain size of 8.6 µm in the flat region and 8.8 µm at the apex of the largest dome.

3.2 Five-Hole Test

Multiaxial five-hole tests were performed on 0.5, 1, and 3-mm thick sheets at six different strain rates: 1×10^{-3}, 8×10^{-4}, 5×10^{-4}, 1.5×10^{-4}, 5×10^{-5}, and 2.4×10^{-5} s^{-1}. Previous discussion illustrated that a suitable target strain rate can result in optimal SPF behavior. As shown in Fig. 2(a), the formed five-hole hemi-spherical domes have different diameters and depths. The achieved five-hole experimental depths for various conditions are listed in Table 2. It should be noted that there were bending effects at the hole edges, and the most severe bending occurred for the thinnest sheet. These effects, however, could be corrected by simple mechanical means before measuring the hole depths. The measured hole depths were used in the simulation program to optimize the material constants, for instance, the modeled initial grain size of the alloy sheet.

Pressure-time profiles of five-hole tests for three different thicknesses of sheet are shown in Fig. 4(a). They were generated by guessing the flow stress and taking into consideration

Table 2 SPF five-hole tests of Ti-6Al-4V alloys at various strain rates (forming temperature 900 °C)

Alloy, mm	Strain rate, s^{-1}	Flow stress, MPa	Forming time, min	Five-hole depth, mm				
				1	2	3	4	5
1	1×10^{-3}	11.64	4.8	3.92	4.97	5.51	6.62	7.31
	8×10^{-4}	10.09	6.0	3.45	4.19	4.73	5.58	5.91
	5×10^{-4}	7.37	9.6	3.62	4.40	4.96	5.93	6.37
	1.5×10^{-4}	3.42	32.0	4.81	5.80	6.38	7.84	8.49
	5×10^{-5}	2.07	95.9	4.37	5.34	5.34	7.20	7.86
	2.4×10^{-5}	0.98	199.8	4.79	5.49	5.50	7.43	8.20
0.5	1×10^{-3}	12.82	4.8	3.71	4.62	5.39	6.31	6.58
	5×10^{-4}	7.87	9.6	3.57	4.27	4.98	6.15	6.76
	1.5×10^{-4}	3.98	32.0	5.58	6.46	7.32	9.14	9.42
	2.4×10^{-5}	1.48	199.8	5.36	6.25	6.96	8.93	9.67
3	1×10^{-3}	12.15	4.8	3.31	4.19	4.32	6.18	7.10
	1.5×10^{-4}	3.97	32.0	5.48	6.98	8.06	9.76	11.01
	2.4×10^{-5}	1.68	199.8	4.84	5.90	6.56	8.28	8.96

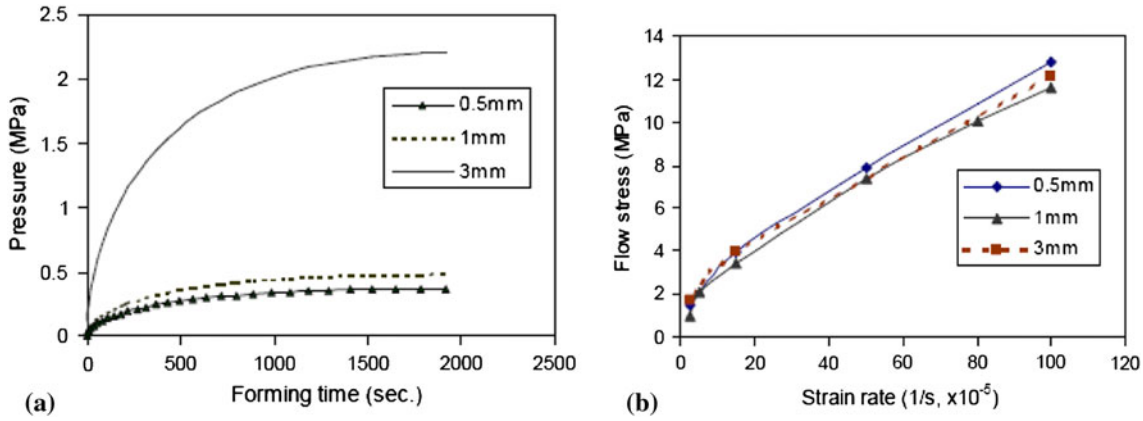

Fig. 4 (a) Pressure-time profile of five-*hole* tests for three different thickness sheets, strain rates 1.5×10^{-5} s^{-1} and (b) calculated flow stress as a function of strain rate for three different thickness sheets

the radius of the middle hole. The established relationship between flow stress and strain rate for the three different sheets is plotted in Fig. 4(b). It is shown that the flow stress increases with increasing strain rate in all sheets with different thickness.

A number of simulations have been attempted to study the strain rate effect on the achieved depth in five holes for 1-mm thick Ti-6Al-4V alloy sheet (see Fig. 5a), and also, the thickness effect on the achieved depth of five holes at constant strain rate (1×10^{-3} s^{-1}, see Fig. 5b). It is observed that the five-hole depth varies according to strain rate, and the depth of the largest hole is achieved at the strain rate of 1.5×10^{-4} s^{-1}. Plots of hole depth versus strain rate for 0.5 and 3 mm alloy sheets also display the same trends, which indicates that the optimum superplasticity can be obtained with proper selection of strain rate for these alloys. The thickness of sheet has a different effect on five-hole depth, and in this context, the largest hole depth was achieved for 1-mm thick sheet at the constant strain rate (1×10^{-3} s^{-1}). Other studies have also shown that the strain rate is a very sensitive factor to the superplasticity of the material (Ref 18, 19), and hence, the appropriate selection of strain rate should be made prior to actual forming of the alloy sheets.

Simulations of five-hole test were carried out using the FE program, predominately using three-node triangular membrane elements, but eight-node hexahedral elements (solid elements) were also used in some cases. In general, a membrane element analysis is suitable for thin sheet which considerably simplifies the formulation in the program, and the software allows automatic mesh refinement during simulation, while solid elements employ one element through the thickness and automatic mesh refinement is not applicable (Ref 18). In all simulations the five-hole steel die was pre-meshed as a standard input file, and the Ti mesh input files were generated for the specific case, i.e., either for membrane elements or solid elements. The triangulated die was represented by 48,665 elements and 24,380 nodes. The Ti mesh input files were modified for each simulation by incorporating the argon gas pressure profile generated for use with the five-hole experiment. For each five-hole experiment, three simulations were carried out using three different estimates of the initial grain size (3, 4, and 5 μm). The simulated initial grain size and the five-hole depths were obtained by interpolation from a best fit between simulation and experiment. The grain size and grain size evolution will be further corroborated by metallographic examination.

Figure 5 shows the simulated external surface of the 1-mm thick Ti sheet at a strain rate of 1.5×10^{-4} s^{-1} using membrane elements and solid element analysis for the same sheet. For membrane analysis, the simulated initial grain size was 2.55 μm. Simulated depths by interpolation and the depths using the measured initial grain size (3.17 μm), as well as the experimental depths from the five-hole tests are shown in Fig. 6(a). It is noted that Fig. 6(a) is plotted using a schematic geometry, neglecting the orientation of the five holes, simply for the convenience of comparing the hole depths in two dimensions. From the comparison of five-hole depths between the experiment and the simulation, one can see that the simulated depths using three guesses of the initial grain size are much closer to the experimental depths than those obtained from simulation using measured initial grain size. The results may have some implications for finding the optimum initial grain size to be input into the FE program. Note that the modeled initial grain size is different from the one obtained from microscopic measurement.

Furthermore, the scatter plot of experimental and simulated five-hole depths for 0.5, 1, 3 mm sheets at six different strain rates (see Table 2) is presented in Fig. 6(b). The standard deviation (RMSE) is 0.36 mm. This statistical analysis indicates that the simulated depths are in good agreement with the experimental ones.

As described above, material characterization is a prerequisite for SPF of Ti-6Al-4V alloys to determine an accurate description of flow stress for FE simulation of dental prostheses. In the Mosher and Dawson constitutive equations which were adopted in the FE Superflag program, all the microstructural variables were correlated with the grain size of the α phase, in other words, the initial grain size of the α phase plays a dominant role in influencing simulation of SPF of Ti alloys. From open literatures associated with superplasticity of titanium alloys, it is also evidenced that strain rate and forming temperature have significant effects on microstructural evolution, such as grain growth, final grain size distribution as well as phase transformation (Ref 12, 17, 20, 21). From this study it has also been shown that the well designed five-hole test, in conjunction with FE simulation, can be used to obtain material information to be used in the practical dental device simulations.

3.3 Simulation of Dental Prosthesis

In order to fabricate Ti alloy dental prostheses by SPF technology, simulation of the SPF processing of dental

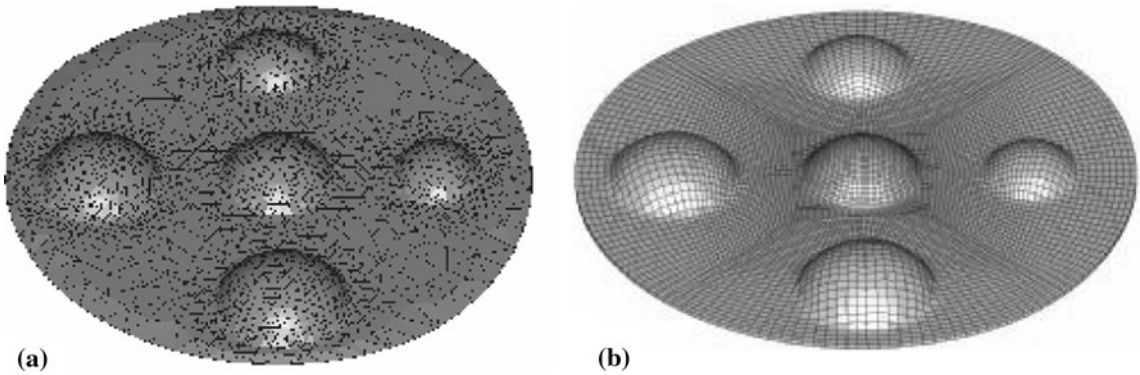

Fig. 5 (a) FE simulation of five-hole test for Ti-6Al-4V sheets, strain rate 1.5×10^{-4} s^{-1}, 1-mm thick, membrane analysis and (b) solid analysis

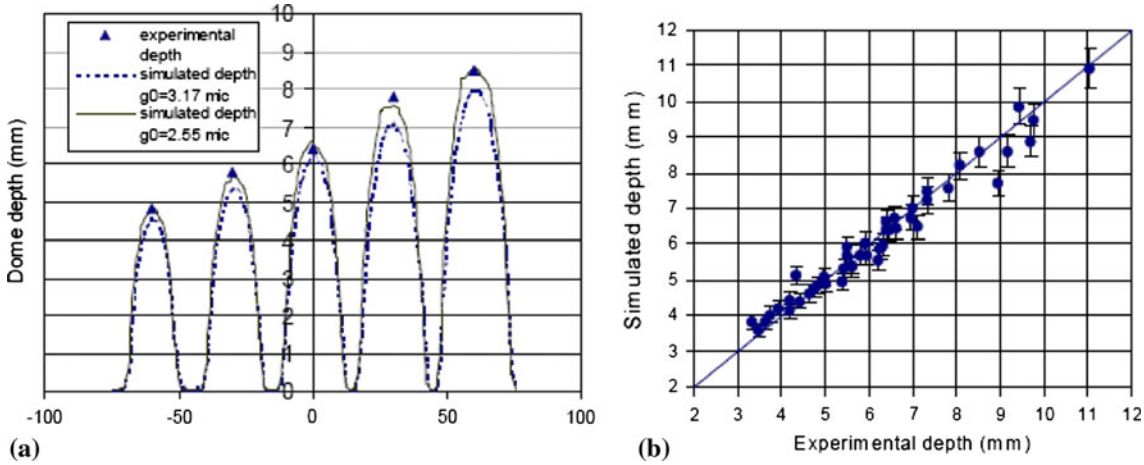

Fig. 6 (a) Comparison of five-hole depths between experiment and simulation and (b) scattered plot of experimental and simulated five-hole depths for 0.5, 1, and 3-mm thick sheets (RMSE: 0.36 mm)

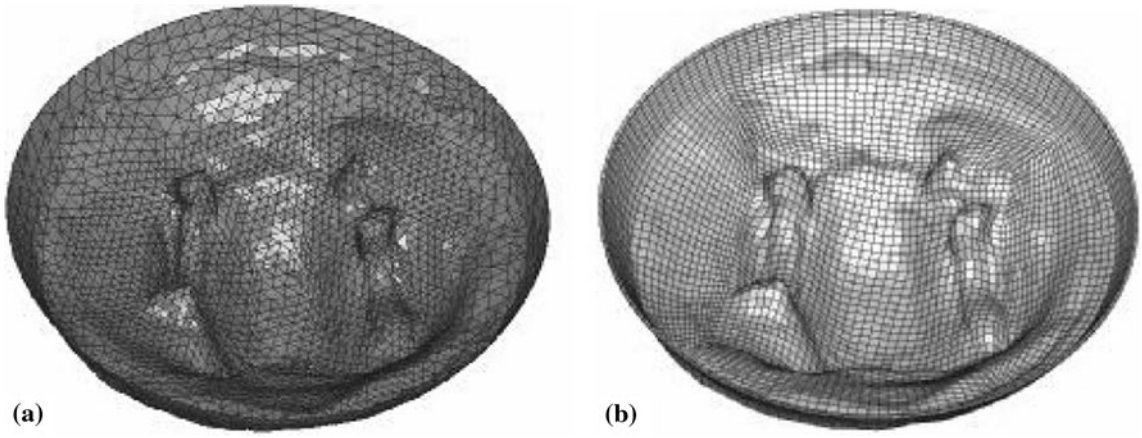

Fig. 7 FE simulation of PUD4 using membrane and solid elements, 0.7-mm thick sheet. (a) Membrane and (b) solid analysis

prostheses is required to generate pressure profiles for download into the control system of the SPF press, once accurate prediction the SPF properties of the material has been proven. The five-hole test was used to obtain a numerical value of the initial grain size which is close to actual initial grain size. Then for any specific strain rate the target flow stress for the pressure cycle prediction algorithm is defined from the constitutive equation. Sticking contact between the sheet and the die surface is required for these simulations of dental prostheses. The die surface definition was obtained from surface reconstruction procedures (see "Surface Reconstruction" section), which is displayed as a triangulated surface. When the surface of the dental master model was scanned, the patches were subsequently processed by artificially deleting spikes and singularities and merged into a triangular meshed shell. Cavities could be present at this stage, and Paraform software, which provided automatic mesh refinement and surface repair, was used to decimate elements and fill any remaining holes to obtain an appropriate mesh for FE simulation. With respect to the Ti mesh input file, both membrane elements and solid elements simulations were carried out. The simulations of a partial upper denture base (PUD4) using both membrane and solid analysis are shown in Fig. 7.

It should be noted that attempts to adopt the target strain rate of 1.5×10^{-4} s^{-1} for simulations of PUD4 resulted in poor contact results, i.e., the thin sheet and the die are apart to an extent that the gap between them can be distinctively discernable. Hence, a number of simulations were undertaken by setting up appropriate target stress or strain rate for membrane and solid analysis. From numerous simulation exercises it has been observed that good simulation results were obtained for PUD4 without setting target stress or strain rate for the membrane analysis, and by setting target stress of 9 MPa for the solid analysis. The predicted parameters obtained from the simulations of PUD4, such as forming time and maximum pressure, are shown in Table 3. Overall, this article attempts to report on the SPF technique and FE simulation applied to dental repair. Other issues related to this study lie in the die geometry, initial thickness selection in terms of thinning process, improvement of the FE program, and further applications in dentistry using SPF technique.

Table 3 Predicted parameters obtained from simulations of PUD4

Parameters	Forming time, s	Maximum pressure, MPa
Membrane	4059	2.06
Solid	5007	2.24

4. Conclusions

SPF of five-hole tests of Ti-6Al-4V alloys and a partial upper denture base of the same alloy were performed at a variety of strain rates. Results showed that optimum superplasticity can be obtained by proper selection of strain rate and thickness of the alloys. Simulations of five-hole test provided the establishment of stress-strain rate relations and the estimate of the modeled initial grain size and a good agreement between the experimental and simulated dome depth is observed. After titanium alloy was characterized and useful parameters were obtained from the five-hole test the dental prosthetic component (partial upper denture base) was satisfactorily simulated using membrane and solid analysis. It is concluded that SPF technique in conjunction with FE simulation can be applied to fabricate dental devices.

Acknowledgments

The authors acknowledge the Engineering and Physical Science Research Council (EPSRC), UK for the financial aid to this work. Drs. R. V. Curtis and A. S. Juszczyk are gratefully acknowledged for their technical help and cooperation.

References

1. M.A. Nazzal, M.K. Khraisheh, and F.K. Abu-Farha, The Effect of Strain Rate Sensitivity Evolution on Deformation Stability During Superplastic Forming, *J. Mater. Proc. Technol.*, 2007, **191**(1–3), p 189–192
2. J. Bonet, A. Gil, R.D. Wood, R. Said, and R.V. Curtis, Simulating Superplastic Forming, *Comput. Methods Appl. Mech. Eng.*, 2006, **195**(48–49), p 6580–6603

3. D. Cheng, J. Huang, X. Zhao, and H. Zhang, Microstructure and Superplasticity of Laser Welded Ti-6Al-4V Alloy, *Mater. Des.*, 2010, **31**(1), p 620–623
4. P. Comley, Manufacturing Advantages of Superplastically Formed Fine-grain Ti-6Al-4V Alloy, *J. Mater. Eng. Perform.*, 2004, **13**(6), p 660–664
5. R.D. Wood, R.V. Curtis, J. Bonet, R. Said, A. Gil, D. Garriga-Majo, and X. Li, Computer Simulation of Superplastic Forming in Restorative Dentistry, *Mater. Sci. Forum*, 2004, **447–448**, p 131–138
6. R.V. Curtis, The Suitability of Dental Investment Materials as Dies for Superplastic Forming of Medical and Dental Prostheses, *Mater. Sci. Eng. Technol.*, 2008, **39**(4–5), p 322–326
7. R.V. Curtis and A. Gil, *Superplastic Forming of Dental and Maxillofacial Prostheses, Dental Biomaterials: Imaging, testing and modelling*, 1st ed., Woodhead Publishing Ltd, Cambridge, UK, 2008, p 428–474
8. D. Garriga-Majo, R.J. Paterson, R.V. Curtis, R. Said, R.D. Wood, and J. Bonet, Optimisation of the Superplastic Forming of a Dental Implant for Bone Augmentation Using Finite Element Simulations, *Dental Materials: Official Publication of the Academy of Dental Materials*, 2004, **20**(5), p 409–418
9. G. Giuliano, Constitutive Equation for Superplastic Ti-6Al-4V Alloy, *Mater. Des.*, 2008, **29**(7), p 1330–1333
10. J. Pilling and N. Ridley, *Superplasticity in Crystalline Solids*, Institute of Metals, Camelot Press plc, Southampton, UK, 1989
11. D.A. Mosher and P.R. Dawson, A State Variable Constitutive Model for Superplastic Ti-6Al-4V Based on Grain Size, *J. Eng. Mater. Technol.*, 1996, **118**, p 162–168
12. J. Cheong, J. Lin, and A.A. Ball, Modeling the Effects of Grain-size Gradients on Necking in Superplastic Forming, *J. Mater. Proc. Technol.*, 2002, **5854**, p 1–9
13. F. Pitt and M. Ramulu, Influence of Grain Size and Microstructure on Oxidation Rates in Titanium Alloy Ti-6Al-4V Under Superplastic Forming Conditions, *J Mater. Eng. Perform.*, 2004, **13**(6), p 727–734
14. A.V. Sergueeva, V.V. Stolyarov, R.Z. Valiev, and A.K. Mukherjee, Superplastic Behaviour of Ultrafine-Grained Ti-6A1-4V Alloys, *Mater. Sci. Eng. A*, 2002, **323**, p 318–325
15. W. Han, K. Zhang, and G. Wang, Superplastic Forming and Diffusion Bonding for Honeycomb Structure of Ti-6Al-4V Alloy, *J. Mater. Proc. Technol.*, 2007, **183**(2–3), p 450–454
16. F.U. Enikeev, Determination of the Value of the Threshold Stress for Superplastic Flow, *Mater. Sci. Eng. A*, 2000, **276**(1–2), p 22–31
17. R.D. Wood and J. Bonet, A Review of the Numerical Analysis of Superplastic Forming, *J. Mater. Proc. Technol.*, 1996, **60**, p 45–53
18. J. Bonet, Error Estimators and Enrichment Procedures for the Finite Element Analysis of Thin Sheet Large Deformation Processes, *Int. J. Numer. Methods Eng.*, 1994, **37**, p 1573–1591
19. H.L. Xing and Z.R. Wang, Finite-Element Analysis and Design of Thin Sheet Superplastic Forming, *J. Mater. Proc. Technol.*, 1997, **68**, p 1–7
20. K.F. Zhang, G.F. Wang, D.Z. Wu, and Z.R. Wang, Research on the Controlling of the Thickness Distribution in Superplastic Forming, *J. Mater. Proc. Technol.*, 2004, **151**(1–3), p 54–57
21. S.G. Luckey, Jr., P.A. Friedman, and K.J. Weinmann, Correlation of Finite Element Analysis to Superplastic Forming Experiments, *J. Mater. Proc. Technol.*, 2007, **194**(1–3), p 30–37